University of Reading

Diagnosing relationships between mean state biases and El Niño shortwave feedback in CMIP5 models

Article

Published Version

It is advisable to refer to the publisher's version if you intend to cite from the work. See Guidance on citing.

www.reading.ac.uk/centaur

Diagnosing Relationships between Mean State Biases and El Niño Shortwave Feedback in CMIP5 Models

SAMANTHA FERRETT AND MATTHEW COLLINS

College of Engineering, Mathematics and Physical Sciences, University of Exeter, Exeter, United Kingdom

HONG-LI REN

Laboratory for Climate Studies, National Climate Center, China Meteorological Administration, Beijing, and Department of Atmospheric Science, School of Environmental Studies, China University of Geoscience, Wuhan, and CMA–Nanjing University Joint Laboratory for Climate Prediction Studies, School of Atmospheric Sciences, Nanjing University, Nanjing, China

ABSTRACT

The rate of damping of tropical Pacific sea surface temperature anomalies (SSTAs) associated with El Niño events by surface shortwave heat fluxes has significant biases in current coupled climate models [phase 5 of the Coupled Model Intercomparison Project (CMIP5)]. Of 33 CMIP5 models, 16 have shortwave feedbacks that are weakly negative in comparison to observations, or even positive, resulting in a tendency of amplification of SSTAs. Two biases in the cloud response to El Niño SSTAs are identified and linked to significant mean state biases in CMIP5 models. First, cool mean SST and reduced precipitation are linked to comparatively less cloud formation in the eastern equatorial Pacific during El Niño events, driven by a weakened atmospheric ascent response. Second, a spurious reduction of cloud driven by anomalous surface relative humidity during El Niño events is present in models with more stable eastern Pacific mean atmospheric conditions and more low cloud in the mean state. Both cloud response biases contribute to a weak negative shortwave feedback or a positive shortwave feedback that amplifies El Niño SSTAs. Differences between shortwave feedback in the coupled models and the corresponding atmosphere-only models (AMIP) are also linked to mean state differences, consistent with the biases found between different coupled models. Shortwave feedback bias can still persist in AMIP, as a result of persisting weak shortwave responses to anomalous cloud and weak cloud responses to atmospheric ascent. This indicates the importance of bias in the atmosphere component to coupled model feedback and mean state biases.

1. Introduction

El Niño–Southern Oscillation (ENSO) is a dominant mode of interannual variability in the equatorial Pacific that has a large impact on weather worldwide. ENSO is driven by a combination of ocean–atmosphere processes that either amplify or damp ENSO-event-related sea surface temperature anomalies (SSTAs) in the equatorial Pacific. Processes that contribute to the growth of initial positive SSTAs in the equatorial Pacific are typically related to ocean processes, such as ocean current anomalies and thermocline anomalies, as a result of decreasing surface zonal winds during El Niño events (the Bjerknes feedback; Bjerknes 1969). Conversely, surface heat fluxes damp the SSTAs (hereafter thermodynamic damping), though ocean dynamics still play a role in event damping. Positive sea surface temperature anomalies increase the vertical specific humidity gradient near the surface, hence increasing evaporation (latent heat feedback). Atmospheric circulation shifts during El Niño events also result in more cloud cover in the east, largely a response to increasing atmospheric ascent, reducing surface downward shortwave radiation (shortwave feedback). These responses have a cooling effect on the initial positive SSTA.

Methods to quantify these ENSO feedbacks are often based on simple linear models of ENSO [e.g., the Bjerknes stability index (BJ index); Jin et al. 2006; Kim and Jin 2011a]. The thermodynamic damping is one of the most dominant of these feedbacks. This is often simply defined as the regression coefficient of east

equatorial Pacific area-averaged surface heat flux anomalies against east Pacific SSTAs. Thermodynamic damping consists of four components corresponding to four surface heat fluxes: latent heat flux, sensible heat flux, shortwave radiation, and longwave radiation. Ultimately, as described above, latent heat flux and shortwave radiation are the largest contributors and drive the ENSO thermodynamic damping (Lloyd et al. 2009). Coupled climate models have been found to struggle to fully capture observational estimates of ENSO characteristics, such as amplitude, spatial structure, and frequency of events (Capotondi et al. 2006; Zhang et al. 2013; Bellenger et al. 2014). Indeed, ENSO-related SSTAs show a great deal of variation in strength among coupled models (Fig. 1a). Thermodynamic damping is one of the main sources of error for ENSO in coupled climate models (Jin et al. 2006; Lloyd et al. 2009; Kim and Jin 2011a; Kim et al. 2014a).

Persistent coupled model biases in the equatorial Pacific mean climate are the cold tongue and double-ITCZ biases (Mechoso et al. 1995; AchutaRao and Sperber 2006; Lin 2007; de Szoeke and Xie 2008; Vannière et al. 2013, 2014; Li and Xie 2014; Zhang et al. 2015). Cooler temperatures along the equator, an indicator of the cold tongue bias, have been linked to the strength of thermodynamic damping during ENSO in coupled climate models (Kim et al. 2014a; Ferrett and Collins 2016). Of particular relevance to shortwave feedback is the established relationship between mean equatorial Pacific sea surface temperatures and the precipitation response during ENSO events (Sun et al. 2006, 2009; Chen et al. 2013). Despite this, a more recent study by Li et al. (2015), which decomposes shortwave feedback in a subset of the most recent generation of coupled climate models (CMIP5; Taylor et al. 2012), was unable to robustly link shortwave feedback variation to other mean climate biases. However, they did note that the vertical distribution of cloud over the equatorial Pacific is different in three CMIP5 models with the strongest negative shortwave feedbacks than those with a weaker negative shortwave feedback (see Fig. 14 of Li et al. 2015). Significant links have been identified between the mean climate in the equatorial Pacific and latent heat feedback in the CMIP5 models (Ferrett et al. 2017). As the strength of latent heat and shortwave (SW) feedback in CMIP5 tend to vary with one another (Fig. 1b), this study aims to highlight any links between the SW feedback bias and mean state bias in coupled models. The atmosphere-only runs (AMIP) are also studied in order to gain further insight into underlying causes of El Niño feedback and mean state bias.

Variation in the strength of ocean–atmosphere processes responsible for ENSO events in coupled climate
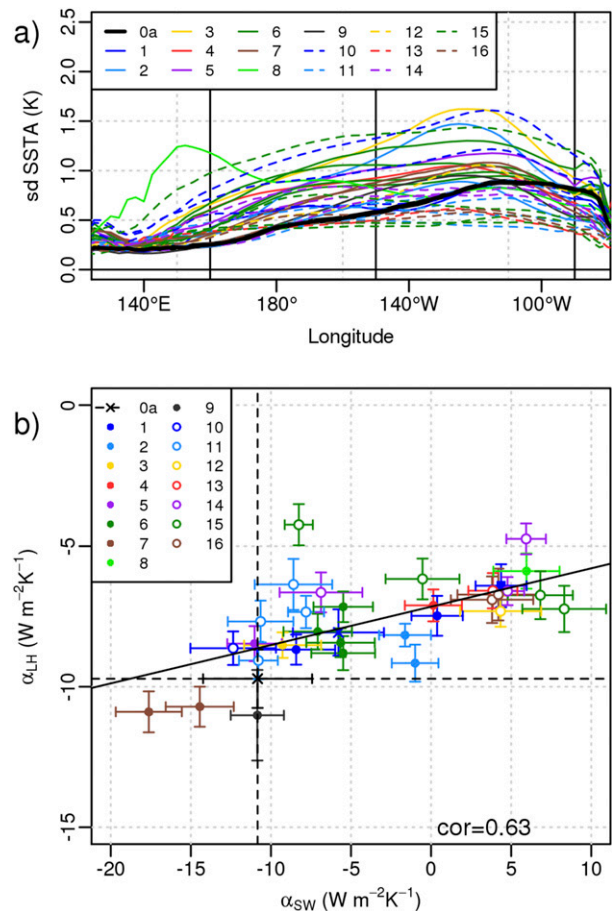

FIG. 1. CMIP5 (a) standard deviation of equatorial mean (averaged over latitude 5°S–5°N) SSTAs as a function of longitude. Niño-4 (160°E–150°W) and Niño-3 (150°–90°W) longitude bounds are shown using vertical black lines, (b) latent heat feedback α_{LH} plotted against El Niño shortwave feedback α_{SW}. Error bars indicate the 95% confidence intervals in the linear fits used in the feedback calculation. Correlations of the relationships for CMIP5 ensemble members are printed on the figure. The fitting line indicates a relationship significant at the 95% level (Student's t test). Model numbers relate to those given in Table 1, and the observational estimates are shown using dashed lines.

models are a significant source of uncertainty in ENSO projections (Sun et al. 2003, 2006; Lloyd et al. 2009, 2012; Kim and Jin 2011b; Kim et al. 2014a,b; Bellenger et al. 2014; Li et al. 2015; Chen et al. 2015, 2017). For example, Kim et al. (2014b) find that using only coupled models that best represent observed ENSO feedbacks results in more robust projections of changes in ENSO amplitude and growth rate in a warming climate. Projections of increasing frequency of extreme ENSO events (Cai et al. 2014) are also based on changes in ENSO-related precipitation anomalies, which are strongly linked to both latent heat and SW processes. Links between mean state biases and ENSO feedback biases ultimately highlight

areas to prioritize in future model development and can help improve confidence in model projections.

Here, the SW feedback decomposition proposed in previous studies (Li et al. 2014, 2015) is used to explore the possible link between common mean state biases (i.e., cold tongue and double-ITCZ biases) and the ocean–atmosphere couplings that drive SW heat flux during El Niño events in the CMIP5 ensemble. The layout of the study is as follows: Details of the CMIP5, AMIP, and observation datasets used are given in section 2. The decomposition of SW feedback used in the analysis is outlined in section 3. Section 4 describes the results of the CMIP5 and AMIP SW feedback analysis and relationships between SW feedback and the equatorial Pacific mean state. A brief summary of the results is given in section 5.

2. Data

a. CMIP5 and AMIP

This study uses historical experiments over the time period 1950–99 for 33 coupled climate models from the World Climate Research Programme (WCRP) CMIP5 multimodel ensemble (Taylor et al. 2012). Details of the models used are given in Table 1 and are chosen based on availability of monthly fields of the required variables. Three-dimensional cloud area fraction is used for a subset of the models, indicated in Table 1. Results from CMIP5 models are also compared to AMIP (Taylor et al. 2012) runs for 15 of the coupled models, indicated in Table 1 by an asterisk by the model name. AMIP analysis is over the time period 1979–2008.

b. Observations and reanalyses

A number of observation and reanalysis datasets are used in comparison to the CMIP5 models. These are ECMWF ERA-Interim (hereafter ERA-I; Dee et al. 2011), objectively analyzed air–sea heat fluxes (OAFlux; Yu and Weller 2007), International Satellite Cloud Climatology Project (ISCCP; Schiffer and Rossow 1983), NCEP–DOE AMIP-II reanalysis (NCEP2; Kanamitsu et al. 2002), Global Precipitation Climatology Project version 2.3 combined precipitation dataset (GPCP; Adler et al. 2003), and Modern-Era Retrospective Analysis for Research and Applications, version 2 (MERRA-2; Gelaro et al. 2017). Shortwave and longwave radiation for OAFlux are provided by ISCCP. Time periods for observations are given in Table 1. Cloud fraction data that may have been used for feedback calculation for Clouds and the Earth's Radiant Energy System (CERES) are not used as the analysis time period is limited enough that there is large uncertainty when linear regression is performed.

3. Methods: El Niño shortwave feedback decomposition

A number of studies highlight biases in the strength of ocean–atmosphere couplings, such as atmospheric circulation and cloud feedbacks, that can be linked to SW feedback bias and variation (Lloyd et al. 2012; Chen et al. 2013; Sun et al. 2009). The SW feedback decomposition method proposed by Li et al. (2014) enables assessment of the relative importance of these couplings to ENSO SW feedback allowing for the isolation of underlying causes of bias. This expands on a decomposition method used by Lloyd et al. (2012) that accounts only for the contribution to shortwave heat flux of processes arising from atmospheric ascent responses to SST. Li et al. (2014) build on this to include processes related to anomalous relative humidity and liquid water path.

El Niño SW feedback, α_{SW}, is calculated by linear regression of downward surface SW heat flux seasonal anomalies, Q_{SW}, averaged over the Niño-3 region (longitude 150°–90°W; latitude 5°S–5°N) on Niño-3 SSTAs, T, such that

$$\alpha_{SW} = \frac{dQ_{SW}}{dT}. \tag{1}$$

Data are detrended prior to calculation, and seasonal anomalies are calculated from monthly fields by removing the mean annual cycle. The decomposition proposed by Li et al. (2014) allows for the separation of the SW feedback into components that represent various atmospheric processes, where

$$\alpha_{SW} = \text{CLDF} + \text{LWPF} = \text{DY} + \text{RHF} + \text{LWPF}. \tag{2}$$

CLDF represents the shortwave heat flux response driven by the response of cloud cover to an SST anomaly:

$$\text{CLDF} = \frac{\partial Q_{SW}}{\partial \text{cld}} \frac{d\text{cld}}{dT}, \tag{3}$$

where $d\text{cld}/dT$ is the response of total cloud cover (cld) to an SSTA, calculated using linear regression. Similarly, $\partial Q_{SW}/\partial \text{cld}$ is the response of the shortwave heat flux to that cloud cover anomaly. The anomalous shortwave heat flux will then affect SST, resulting in a feedback loop. These terms calculated over Niño-3 are referred to as El Niño feedbacks; CLDF is here named the cloud feedback. CLDF can be further split into a dynamical cloud feedback (DY), representing the response of the effects of atmospheric ascent at 500 hPa, ω_{500}, on cloud cover, and therefore SW heat flux, and a surface relative humidity (rh) cloud feedback (RHF):

TABLE 1. Table of model names used in this study. Both atmosphere-only and coupled versions are analyzed. Models used in atmosphere-only analysis are indicated using an asterisk. Models with ISSCP-simulator variables are indicated in bold. Note that three-dimensional cloud was not available for models 1a, 1b, 7a, 7b, 9, 12, and 15c.

No.	Name	Modeling center/notes
0a	OAFlux/ISCCP	Provides shortwave heat flux, cloud area fraction; 1984–2007
	GPCP	Precipitation; 1980–2009
	ERA-Interim	SST, LWP, ω_{500}, relative humidity; 1984–2007
0b	NCEP2	1984–2009
0c	MERRA-2	1984–2009
1a	ACCESS1.0*	CSIRO and Bureau of Meteorology (BOM), Australia
1b	ACCESS1.3*	
2a	BCC_CSM1.1	Beijing Climate Center, China Meteorological Administration
2b	BCC_CSM1.1(m)	
3	BNU-ESM*	College of Global Change and Earth System Science, Beijing Normal University
4	**CanESM2**	Canadian Centre for Climate Modelling and Analysis
5	CCSM4*	National Center for Atmospheric Research
6a	CESM1(BGC)	Community Earth System Model contributors
6b	CESM1(CAM5)*	
6c	CESM1(FASTCHEM)	
6d	CESM1(WACCM)	
7a	CNRM-CM5*	Centre National de Recherches Météorologiques/Centre Européen de Recherche et
7b	CNRM-CM5–2	Formation Avancée en Calcul Scientifique
8	CSIRO Mk3.6.0*	Commonwealth Scientific and Industrial Research Organization in collaboration with Queensland Climate Change Centre of Excellence
9	FGOALS-g2	LASG, Institute of Atmospheric Physics, Chinese Academy of Sciences, and CESS, Tsinghua University
10a	GFDL CM3*	NOAA/Geophysical Fluid Dynamics Laboratory
10b	GFDL-ESM2G	
10c	GFDL-ESM2M	
11a	GISS-E2-H	NASA Goddard Institute for Space Studies
11b	GISS-E2-H-CC	
11c	GISS-E2-R	
11d	GISS-E2-R-CC	
12	**HadGEM2-ES***	Met Office Hadley Centre (additional realizations contributed by Instituto Nacional de Pesquisas Espaciais)
13	INM-CM4.0*	Institute for Numerical Mathematics
14a	IPSL-CM5A-LR*	L'Institut Pierre-Simon Laplace
14b	IPSL-CM5A-MR*	
14c	IPSL-CM5B-LR*	
15a	**MIROC-ESM**	Japan Agency for Marine-Earth Science and Technology, Atmosphere and Ocean Research
15b	**MIROC-ESM-CHEM**	Institute (University of Tokyo), and National Institute for Environmental Studies
15c	MIROC4h	Atmosphere and Ocean Research Institute (University of Tokyo), National Institute for
15d	**MIROC5***	Environmental Studies, and Japan Agency for Marine-Earth Science and Technology
16a	**MRI-CGCM3***	Meteorological Research Institute
16b	MRI-ESM1	

$$\text{DY} = \frac{\partial Q_{\text{SW}}}{\partial \text{cld}} \frac{\partial \text{cld}}{\partial \omega_{500}} \frac{d\omega_{500}}{dT} \quad \text{and} \qquad (4)$$

$$\text{RHF} = \frac{\partial Q_{\text{SW}}}{\partial \text{cld}} \frac{\partial \text{cld}}{\partial \text{rh}} \frac{d\text{rh}}{dT}. \qquad (5)$$

Note that the pressure tendency anomaly at 500 hPa, ω_{500}, is used; therefore, negative ω_{500} corresponds to atmospheric ascent. Shortwave heat flux is also strongly linked to cloud liquid water path, the column amount of liquid water in the cloud, as this determines cloud optical thickness. Therefore, the contribution of anomalous liquid water in clouds to shortwave heat flux feedback (LWPF) is given as

$$\text{LWPF} = \frac{\partial Q_{\text{SW}}}{\partial \text{lwp}} \frac{d\text{lwp}}{dT}. \qquad (6)$$

In the text $d\omega_{500}/dT$, $\partial \text{cld}/\partial \text{rh}$, and $d\text{lwp}/dT$ are referred to as the ω_{500}–SST coupling, the cloud–RH coupling, and the LWP–SST coupling, respectively. See also Eqs. (2) and (3) of Li et al. (2014) for the SW feedback decomposition into DY, RHF, and LWPF components. This study focuses on all components, unlike in Li et al. (2014) where the focus was mainly on total cloud, dynamical, and LWP feedbacks. This has allowed for greater insight into the SW feedback bias, in relation to the mean state bias.

Studies that quantify shortwave feedback using linear regression must account for the nonlinearity of the shortwave heat flux in response to SSTAs (Lloyd et al. 2012; Bellenger et al. 2014). The assumption of linearity is not always valid as the shortwave response during ENSO events can be asymmetric. During an El Niño, a positive SST anomaly in a region of atmospheric ascent results in an increase in convective clouds, reducing the shortwave radiation reaching the surface (Ramanathan and Collins 1991). However, during the ENSO cool phase, La Niña, a decrease in SST can increase both the static stability in the atmospheric boundary layer and the amount of stratiform clouds (Klein and Hartmann 1993; Philander et al. 1996), also decreasing the shortwave heat flux at the surface. This observed nonlinearity (i.e., less downward surface SW during both El Niño and La Niña) also tends not to be fully captured in coupled climate models (Lloyd et al. 2012; Bellenger et al. 2014). As a consequence of this nonlinear behavior, it is more appropriate to separately consider the feedback during El Niño and La Niña events (e.g., Lloyd et al. 2012; Bellenger et al. 2014; Li et al. 2015). This is opposed to assuming a linear relationship between anomalous shortwave heat flux and SSTA over both El Niño and La Niña events. Here, the focus will be only on assessing the feedback on positive SSTAs (El Niño) in CMIP5. Study of La Niña–only feedbacks gave very similar results when relating variations of SW feedbacks to the mean state, so these results have been omitted. To obtain a feedback during El Niño events only, linear regressions are calculated using positive Niño-3 SSTAs ($T > 0$ K). We note that using a different threshold for feedback calculation, such as $T > 0.5$ K, results in feedbacks not significantly different from those calculated for positive T. Similarly, results are found to be relatively insensitive to the choice of boundaries for area averaging. Feedbacks calculated using these alternatives are found to be highly correlated with those calculated using the methods in this study.

Error bars for feedbacks are based on the 95% confidence interval for the linear least squares regression fits used in the calculation of the couplings. This is calculated using the linear fit standard error and the 97.5th percentile of the Student's t distribution.

4. Results

a. ENSO SSTAs and El Niño shortwave feedback in CMIP5

The standard deviation of SSTAs can be used to indicate the strength and zonal location of El Niño/La Niña events along the equator (Fig. 1a). In reanalyses, SSTAs are strongest in the east equatorial Pacific. This peak in the east Pacific is present in many of the CMIP5 models but can occur at different strengths. Some models feature a larger peak in the Niño-3 region than in observations (e.g., BNU-ESM, GFDL-ESM2M, and MIROC5). However, others (e.g., MIROC4h and CSIRO Mk3.6.0) have SSTA peaks located toward the west equatorial Pacific. Generally, models used in this study display a range of SSTA variability in the east equatorial Pacific with little consistent bias in the strength. Other characteristics of ENSO, such as frequency, in CMIP5 models show similar variation (Bellenger et al. 2014).

SW feedback and the three components, DY [Eq. (4)], RHF [Eq. (5)], and LWPF [Eq. (6)], calculated for CMIP5 and two sets of observations are shown in Fig. 2. The reanalyses, ERA-I/OAFlux (marked 0a), NCEP2 (marked 0b), and MERRA-2 (marked 0c), have SW feedback during El Niño events that is negative with strengths of -10.8 ± 3.4, -6.4 ± 2.7, and -13.6 ± 3.8 W m^{-2} K^{-1}, respectively (i.e., surface SW fluxes damp the positive El Niño SST anomalies). The SW feedback is also mostly driven by DY processes that have a strength of -11.5 W m^{-2} K^{-1} in ERA-I/OAFlux, -5.8 W m^{-2} K^{-1} in NCEP2, and -8.0 W m^{-2} K^{-1} in MERRA-2 (Figs. 2a,b).

SW feedback strength tends to vary a relatively large amount throughout the CMIP5 ensemble. In comparison to ERA-I/OAFlux, 16 models have significantly weak negative SW feedback (outside of the observational 95% confidence intervals), and 8 models even have positive SW feedback. A positive SW feedback demonstrates an increase in surface downward shortwave radiation during El Niño events, increasing the initial SST anomaly. Many of the CMIP5 models have a weak negative dynamical feedback in comparison to observations. This is shown to be the most consistent source of bias with 23 CMIP5 models having DY significantly weaker than the observed (ERA-I/OAFlux) feedback (Fig. 2b). This is in agreement with previous studies that find this to be a persistent bias of coupled climate models (Lloyd et al. 2012; Chen et al. 2013; Li et al. 2015). The number of biased models is reduced when comparing CMIP5 with NCEP2 (0b) as the NCEP2 SW feedback and DY are somewhat weaker than ERA-I/OAFlux. This demonstrates the uncertainty that exists between the reanalyses.

The remaining two feedbacks are somewhat smaller in observations (ERA-I/OAFlux has -0.1 and 0.6 W m^{-2} K^{-1} for RHF and LWPF, respectively) though still tend to vary in strength in the CMIP5 ensemble (Figs. 2c,d). LWPF is strongly negative in 12 of the CMIP5 models. This counteracts the DY bias in these models, resulting in a SW feedback closer to the observed strength that is
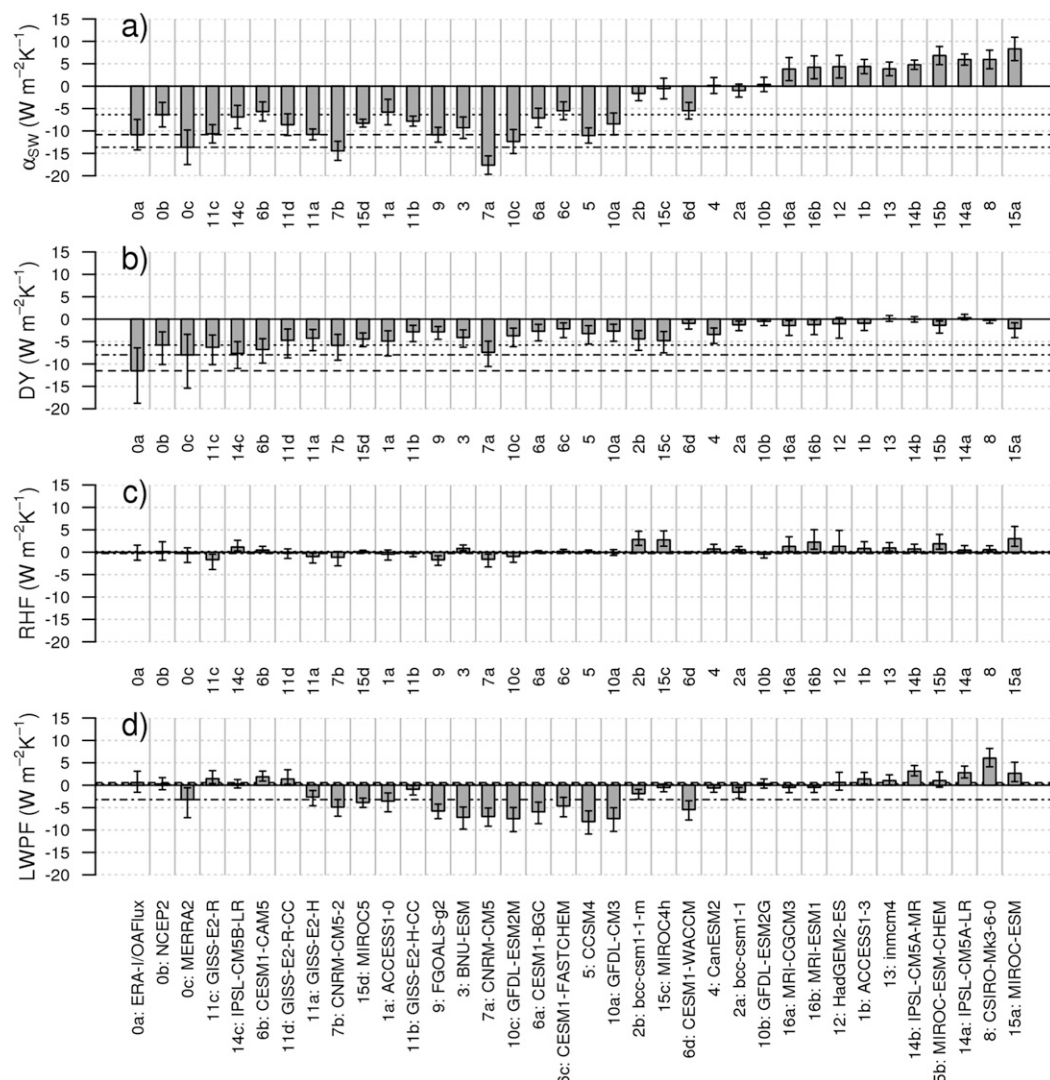
FIG. 2. CMIP5 El Niño (a) shortwave feedback (regression of Niño-3 Q_{SW} anomalies against Niño-3 SSTA for SSTA > 0), (b) DY, (c) RHF, and (d) LWPF. Error bars indicate the 95% confidence intervals in the linear fits used in the feedback calculation. CMIP5 models are ordered by the root-mean-square error of SW feedback, DY, RHF, and LWPF with the 0a feedbacks. Estimates from observations are also given and are shown by dashed (ERA-I/OAFlux), dotted (NCEP2), and dot–dashed (MERRA-2) horizontal lines.

more driven by the liquid water path response. Therefore, models that have more accurate SW feedback may still have underlying feedback errors. In the models with positive SW feedback, DY is closer to zero and both RHF and LWPF are strongly positive. The sum of the individual components can be different compared to SW damping calculated using the model shortwave heat flux field. However, SW damping given by the sum of the components is not significantly different from that calculated using the shortwave heat flux field for any of the CMIP5 models, when taking into account the 95% confidence intervals of the linear fits. As such, differences between the SW feedback and the sum of the

components can be accounted for by the uncertainty in the linear regression analysis. Biases such as those shown in Fig. 2 may be indicative of spatial biases in the feedbacks. This is examined in more detail later.

Although DY dominates SW feedback in observations, the weaker feedbacks, RHF and LWPF, are still of importance when assessing model bias or the variation of SW feedback strength within an ensemble (Fig. 2). SW feedback variation among CMIP5 models is strongly related to variation in the cloud cover response to SSTAs (Fig. 3a; correlation of −0.93). SW feedback bias is largely a result of negative bias in the cloud–SST coupling. The cloud–SST coupling is important to both
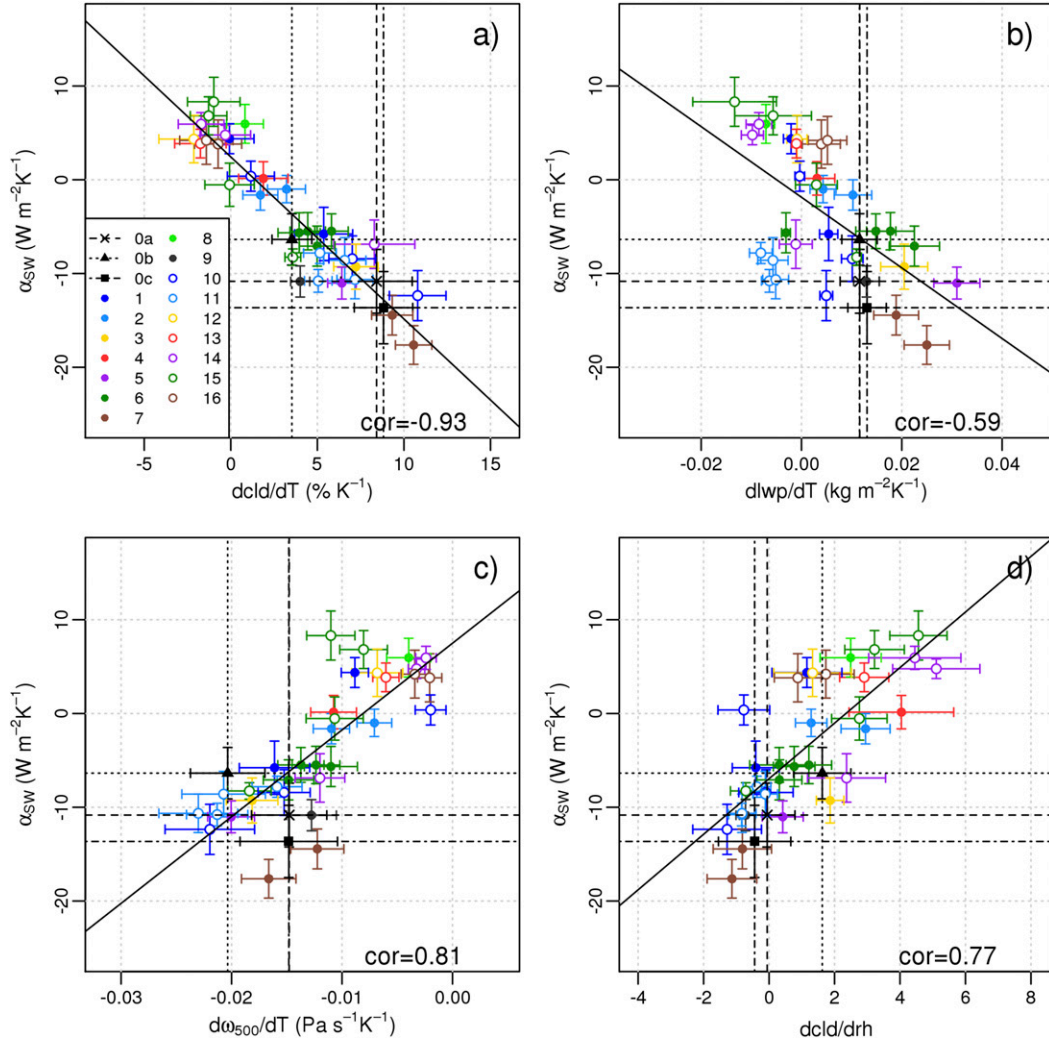
FIG. 3. CMIP5 El Niño shortwave feedback plotted against (a) cloud–SST coupling, (b) LWP–SST coupling, (c) ω_{500}– SST coupling, and (d) cloud–RH coupling. Error bars indicate the 95% confidence intervals in the linear fits used in the feedback calculation. Correlations of the relationships for CMIP5 ensemble members are printed on figures. The fitting line indicates a relationship significant at the 95% level (*t* test). Observational estimates are shown by dashed (ERA-I/OAFlux), dotted (NCEP2), and dot–dashed (MERRA-2) lines.

relative humidity cloud and dynamical cloud feedbacks and contains a relative humidity component and an atmospheric ascent component [Eqs. (4) and (5)].

Variations in both RHF and DY components among CMIP5 models contribute to SW feedback variation (Figs. 3c,d). Significant positive correlations are found between SW feedback and the ω_{500}–SST coupling (correlation of 0.81) and the cloud–RH coupling (correlation of 0.77). The relationship between SW feedback and the cloud–RH coupling suggests that, although RHF tends to be smaller in magnitude than DY and LWPF, it is still linked to the variation of SW feedback strength between models (see Table 2 also). It is also noted that while the total SW feedback components

(DY, RHF, and LWPF) are not strongly related to one another, certain ocean–atmosphere couplings that contribute to each of the components are in fact related. The cloud–RH coupling varies with the ω_{500}–SST coupling, as well as LWPF (Table 2). Models with a strong positive cloud response to relative humidity anomalies and a positive ω_{500}–SST coupling bias tend to be models with a larger positive SW feedback bias. Finally, a component of LWPF is also related to variation in the strength of SW feedback among models. A relatively weak, but still significant, correlation of −0.59 exists between SW feedback and the LWP–SST coupling (Fig. 3b).

A study of CMIP3 models found that damping by SW flux was larger in models with weaker ENSO events

TABLE 2. Correlations between Niño-3 (N3) CMIP5 std dev of SSTA (ENSO amplitude), SW feedback, DY, RHF, LWPF, ω_{500}–SST coupling $d\omega_{500}/dT$, cloud–relative humidity coupling $\partial\mathrm{cld}/\partial\mathrm{rh}$, and liquid water path–SST coupling $d\mathrm{lwp}/dT$. Correlations significant at 95% level by a Student's t test are in bold.

	Std dev N3 SSTA	SW	DY	RHF	LWPF	$\dfrac{d\omega_{500}}{dT}$	$\dfrac{\partial\mathrm{cld}}{\partial\mathrm{rh}}$
SW	**−0.48**	SW					
DY	−0.21	**0.72**	DY				
RHF	−0.22	**0.73**	0.29	RHF			
LWPF	**−0.65**	**0.74**	0.32	**0.42**	LWPF		
$\dfrac{d\omega_{500}}{dT}$	−0.39	**0.81**	**0.65**	**0.50**	**0.58**	$\dfrac{d\omega_{500}}{dT}$	
$\dfrac{\partial\mathrm{cld}}{\partial\mathrm{rh}}$	−0.27	**0.77**	**0.41**	**0.73**	**0.57**	**0.59**	$\dfrac{\partial\mathrm{cld}}{\partial\mathrm{rh}}$
$\dfrac{d\mathrm{lwp}}{dT}$	**0.59**	**−0.59**	−0.27	−0.28	**−0.86**	−0.34	**−0.41**

(Lloyd et al. 2012). However, a more recent study on a subset of CMIP5 models found no obvious relationship between the two (Chen et al. 2013). Here, a slightly stronger relationship between SW feedback and ENSO amplitude is found compared with that shown by Chen et al. (2013), and is in contrast to the positive relationship found by Lloyd et al. (2012) (see Table 2). However, it is still relatively weak (correlation of −0.48) and only persists for LWPF (correlation of −0.65). The remaining two components, DY and RHF, have insignificant relationships with ENSO amplitude. This is most likely due to contributions of other feedbacks to the strength of El Niño events [e.g., as demonstrated by ENSO stability studies such as Kim and Jin (2011a,b)]. These weak relationships also suggest that significant differences can exist between modeled atmospheric responses to equivalent-strength El Niño SSTAs.

Variation in El Niño feedbacks can be a result of spatial biases, both in the mean climate and in El Niño responses. This is demonstrated by the feedbacks in Fig. 4 plotted against longitude over the equatorial Pacific. In observations, the shortwave response to Niño-3 SSTAs peaks in the central equatorial Pacific and is negative east of approximately 170°E (Fig. 4a). This demonstrates a decrease in the downward surface shortwave radiation in these regions during El Niño, cooling the SST there. Some of the CMIP5 models replicate the spatial pattern of this damping well; however, others have spatial biases. Calculating spatial correlations of α_{SW} (shortwave heat flux regressed on Niño-3 SSTA) over the tropical Pacific with the observed α_{SW} finds that 14 of the CMIP5 models have a spatial correlation less than 0.6 (not shown in figures). A correlation below this level also indicates that the CMIP5 model has a larger bias in Niño-3 SW feedback, with a value above $-1.0\,\mathrm{W\,m^{-2}\,K^{-1}}$ (the value corresponding to BCC_CSM1.1 in Fig. 2). SW feedback in CMIP5 can be too strongly positive in the east equatorial Pacific compared with observations, indicating

increasing SW flux during El Niño events, warming the SST. Some CMIP5 models also have a westward-shifted shortwave El Niño response compared with the observed response that consequently results in weaker negative, or positive, SW feedback in the east.

The CMIP5 ω_{500}–SST coupling has similar spatial biases to those of the SW feedback (Fig. 4b). This suggests this is the main driver of the westward-shifted SW feedback in Fig. 4a. It is possible this is a result of the persistent coupled climate model cold tongue bias, characterized by cool temperatures along the equator, which result in a westward shift of El Niño–related SST variance, as well as a westward shift of the ascending branch of the Walker circulation in the mean state. This means that the atmospheric response during El Niño will also tend to be shifted westward, hence weakening the ω_{500}–SST coupling in the east equatorial Pacific. This possible link between ω_{500}–SST coupling and the cold tongue bias is assessed in section 4b.

The spatial distribution of the other dominating component, cloud–RH coupling, is shown in Fig. 4c. During El Niño events, a negative RH anomaly exists in response to positive SSTA. In this case, observations have a negative cloud–RH coupling toward the west equatorial Pacific, corresponding to increasing cloud there during El Niño events, and therefore reduced SW. Conversely, there is a positive response to anomalous surface RH toward the east Pacific. Some models have a positive coupling in the east that is too strong, and this, in combination with weak ω_{500}–SST coupling (Fig. 4b), results in a significantly positive Niño-3 SW feedback for 10 CMIP5 models; both MIROC-ESM models, both IPSL-CM5A models, both MRI models, CSIRO Mk3.6.0, INM-CM4.0, ACCESS1.3, and HadGEM2-ES (Figs. 4a and 2a). CMIP5 models can also have a cloud–RH coupling spatial pattern in contrast to observations that contributes to a negative SW feedback. These models tend to have a negative coupling in the east Pacific
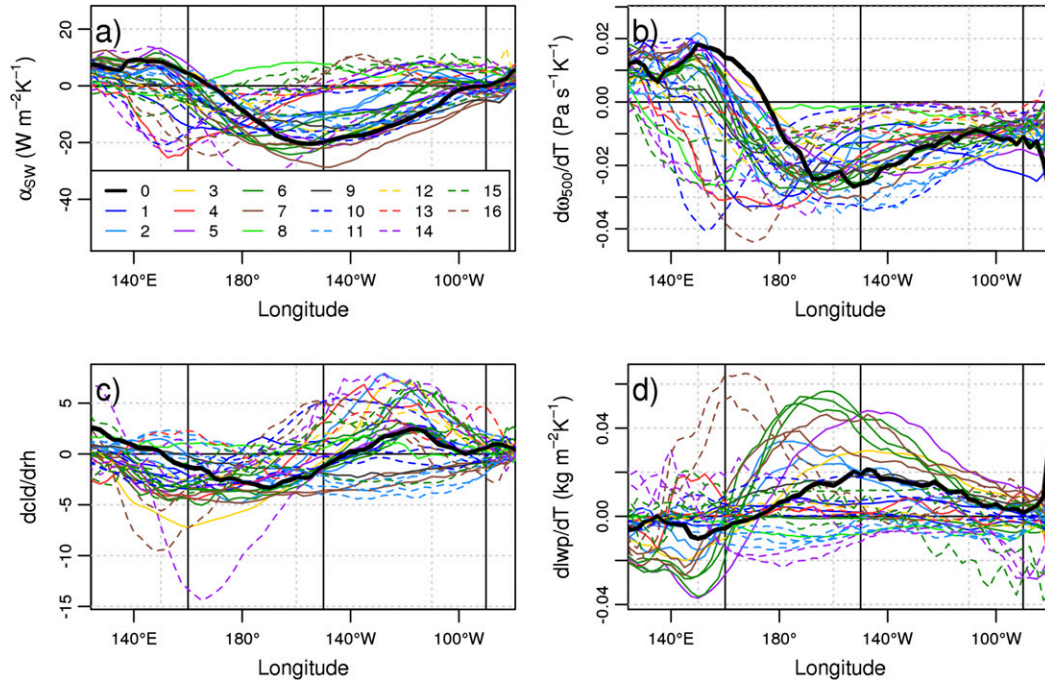
FIG. 4. (a) CMIP5 and observed SW feedback (shortwave radiation heat flux seasonal anomalies regressed on Niño-3 SSTA) as a function of longitude, averaged over latitude 5°S–5°N; (b) as in (a), but for ω_{500}–SST coupling (atmospheric ascent seasonal anomalies regressed on Niño-3 SSTA); (c) as in (a), but for cloud–RH coupling (total cloud cover seasonal anomalies regressed on Niño-3 surface relative humidity anomalies); (d) as in (a), but for LWP–SST coupling (cloud liquid water path seasonal anomalies regressed on Niño-3 SSTA). Niño-3 (longitude 150°–90°W) and Niño-4 (longitude 160°E–150°W) regions are shown using vertical black lines. CMIP5 results are shown using colored solid and dashed lines; observations (ERA-I/OAFlux) are shown using a thick solid black line. All regressions are calculated for SSTA > 0.

and a more positive coupling in the west Pacific (Fig. 4c). Twelve CMIP5 models have a negative Niño-3 cloud–RH coupling (Fig. 3d).

The observed LWP–SST coupling has a positive peak in the central equatorial Pacific, demonstrating an increased optical thickness of the clouds there during El Niño (Fig. 4d). Similar to the cloud–RH coupling, models show large variance in the sign of this coupling. There are also large positive biases in the west equatorial Pacific, with westward shifts in some models' peak LWP–SST coupling. As a result of these biases, 4 CMIP5 models have significantly strong LWP–SST coupling in Niño-3 and 20 models have significantly weak LWP–SST coupling in Niño-3. The westward shift of LWP variability in some models appears of a similar nature to the biases of both SW feedback and the ω_{500}–SST coupling, despite the weaker relationship LWP–SST coupling has with SW feedback (Fig. 3).

These coupling biases and variation are further investigated by assessing any relationship they may have with the mean state, known to be linked to ENSO-related ocean–atmosphere couplings (e.g., Guilyardi et al. 2009; Kim et al. 2014a; Ferrett and Collins 2016; Ferrett et al. 2017).

b. Relationships between coupled model mean climate and shortwave feedback processes

Variations in SW feedback among the CMIP5 models basically demonstrate two regimes of the SW feedback. The first is a negative regime dominated by a negative dynamical feedback and, in some CMIP5 models, negative liquid water path feedback; that is, a positive SSTA induces atmospheric ascent, and convective clouds form and reduce the downward surface SW flux (Ramanathan and Collins 1991). Models with a negative SW feedback have stronger positive cloud feedbacks at higher altitudes in the Niño-3 region (Fig. 5b). The second is a positive regime, not present in the east equatorial Pacific during observed El Niños, that is demonstrated by weak dynamical cloud feedback and positive relative humidity and liquid water path feedbacks. A positive SSTA can decrease static stability, breaking up stratiform clouds and increasing SW flux (Klein and Hartmann 1993; Philander et al. 1996). Models with positive SW feedbacks have a negative cloud feedback at lower altitudes in the Niño-3 region that is not present in models with negative SW feedbacks
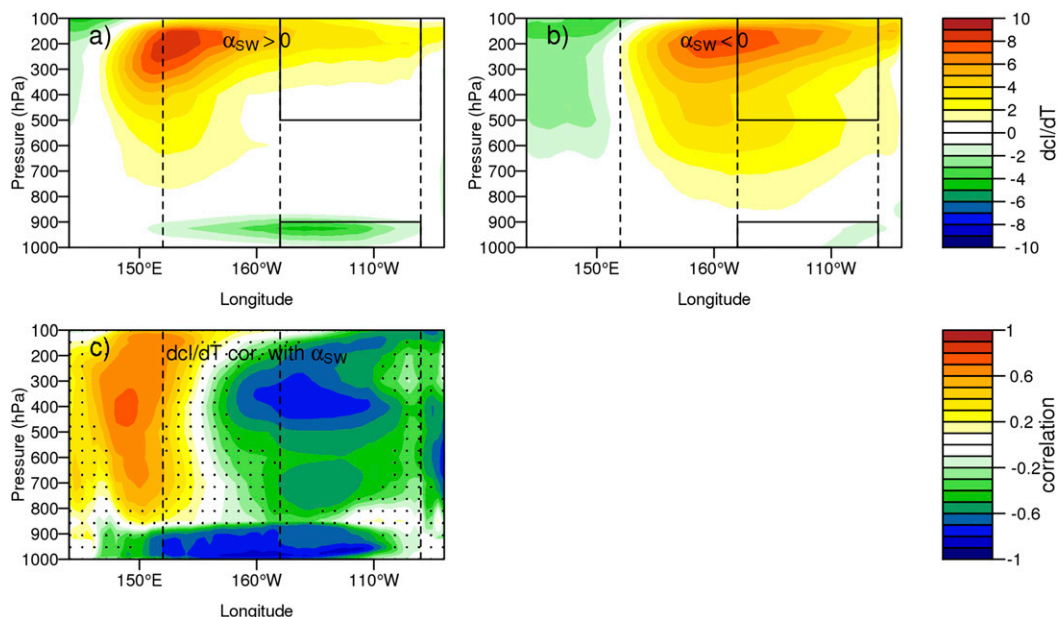
FIG. 5. (a) Cloud fraction seasonal anomalies (%; averaged over latitude 5°S–5°N) regressed onto Niño-3 SSTAs (cloud feedback) for CMIP5 models with positive Niño-3 SW feedback; (b) as in (a), but for CMIP5 models with negative SW feedback; (c) correlation of CMIP5 cloud feedback (averaged over latitude 5°S–5°N) at each grid point with CMIP5 Niño-3 SW feedback. Regions where correlation is below 95% significance (t test) are stippled. Niño-3 and Niño-4 regions are shown using vertical dashed lines. Boxed regions in (a) and (b) show the high (500–100 hPa) and low cloud (1000–900 hPa) regions for the high and low cloud feedback calculation.

(Fig. 5a). Furthermore, variation in the SW feedback can be significantly linked to these variations in cloud feedbacks at different altitudes (Fig. 5c) such that models with a more positive SW feedback have reduced Niño-3 high cloud feedback and more negative low cloud feedback. This is shown by significant negative correlations in these regions between Niño-3 surface SW feedback and cloud feedback. This is also confirmed by examining the relationship of the SW feedback with area-averaged Niño-3 low cloud (pressure 1000–900 hPa) feedback and Niño-3 high cloud (500–100 hPa) feedback. Correlations of −0.81 and −0.71 are found between the SW feedback and low cloud and high cloud feedbacks, respectively (Fig. 6).

The variation among the CMIP5 models between two SW feedback regimes is also supported by the link found between CMIP5 ω_{500}–SST coupling and cloud–RH coupling (Table 2; correlation of 0.59). A model with a more negative ω_{500}–SST coupling tends to also have more negative cloud–RH coupling and vice versa. SW feedback is dominated by either a negative regime or a positive regime. Both regimes are linked to background conditions, either allowing convection to occur or having more stable atmospheric conditions where stratiform clouds are present. This is shown by the relationships between SW feedbacks and the equatorial Pacific mean climate in Fig. 7. Mean states in Fig. 7 are

mainly averaged over the Niño-3 region, as this is the region in which the SW feedback is calculated.

The cloud–RH coupling is linked to mean Niño-3 surface relative humidity (correlation of 0.59; Fig. 7a), such that CMIP5 models with higher mean surface relative humidity in the equatorial Pacific have a stronger positive cloud–RH coupling. This relationship also exists with Niño-4 mean relative humidity (correlation of 0.64), indicating that relative humidity across the full equatorial Pacific basin is important. Models with higher mean surface relative humidity, and the strongest positive cloud–RH couplings (Fig. 7a), may then have a positive SW feedback (Fig. 7e). Models with higher surface relative humidity demonstrate conditions associated with low cloud cover, that is, strong mean atmospheric descent, cool mean surface temperatures, and higher tropospheric static stability (assessed using potential temperature θ at 700 hPa minus θ at the surface; not shown in figures). These conditions would tend toward a positive SW feedback regime, described above and shown in Fig. 5a, and are shown here by a stronger positive cloud–RH coupling. The vertical distribution of cloud is therefore an area of interest in order to confirm that this is indeed an underlying driver of the relationships shown in Fig. 7a and Fig. 7e. This is assessed later.

Aspects of the cold tongue bias, such as mean sea surface temperature and equatorial Pacific precipitation,
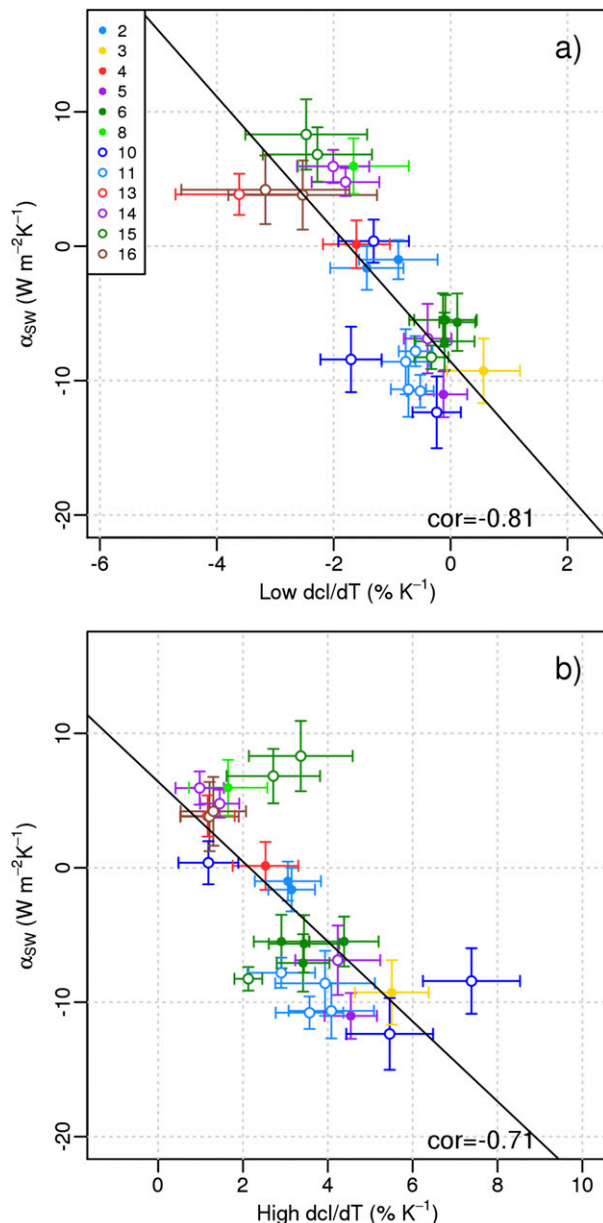
FIG. 6. (a) CMIP5 Niño-3 SW feedback plotted against CMIP5 Niño-3 low cloud (pressure 1000–900 hPa) feedback; (b) as in (a), but with CMIP5 Niño-3 high cloud (pressure 500–100 hPa) feedback on the *x* axis. Error bars indicate the 95% confidence intervals in the linear fits used in the feedback calculation. Correlations of the relationships for CMIP5 ensemble members are printed on figures. The fitting line indicates a relationship significant at the 95% level (*t* test).

can also be linked to dominant SW feedback components, as shown in Fig. 7. Figures 7b and 7c show negative correlations between the ω_{500}–SST coupling and mean Niño-3 temperature and Niño-3 precipitation with correlations of −0.61 and −0.60, respectively. The ω_{500}–SST coupling is also significantly correlated with mean Niño-4

precipitation (correlation of −0.67) and mean Niño-3 and Niño-4 atmospheric ascent (correlations of 0.55 and 0.62, respectively; not shown in figures). These relationships demonstrate that models with cooler temperatures, less precipitation, and less atmospheric ascent in the equatorial Pacific have more precipitation to the far west outside of the Niño-4 region and have weaker atmospheric ascent anomalies in response to SSTAs during El Niño events. Ultimately, the reduced atmospheric ascent anomalies mean less convective cloud cover is formed during El Niño events (via cloud–ω_{500} coupling) and so surface shortwave radiation is not as strongly reduced (via Q_{SW}–cloud coupling). As the ascending branch of the Walker circulation in the mean state tends to be shifted toward the west in models with a larger cold tongue bias, this also shifts the atmospheric ascent response westward (Fig. 4b). This then reduces the feedback in the east equatorial Pacific where damping by SW heat flux is most influential to El Niño events. Therefore, models with a larger cold tongue bias and westward-shifted precipitation tend to have reduced negative SW feedback (Figs. 7f,h). Note that the relationships between SW feedback and the cold tongue bias are somewhat less strong than that with the mean relative humidity. Despite the significant relationship between mean precipitation and the ω_{500}–SST coupling, we also note that Niño-3 precipitation is not strongly linked to the total SW feedback (Fig. 7g). It is possible this is a result of SW feedback variation being more strongly related to relative-humidity-related processes, and mean Niño-4 precipitation is linked to mean surface relative humidity (correlation of −0.83). However, Niño-3 precipitation is not. Niño-4 is also a better measure of spatial bias in the Walker circulation, given the proximity of the ascending branch of the circulation to Niño-4 compared with Niño-3.

Last, the less dominant LWP–SST coupling can be linked to Niño-3 total cloud cover (Fig. 7d). Cloud liquid water path depends on both cloud amount and in-cloud liquid water content; Li and Zhang (2008) link weak LWP–SST coupling in NCAR CAM3 to both weak cloud anomalies and weak in-cloud liquid water anomalies. Here, the relationship between LWP–SST coupling and mean Niño-3 cloud cover indicates that a higher level of mean cloud cover in the east Pacific tends to result in a more negative LWP–SST coupling. A positive relationship exists between LWP–SST coupling and cloud–SST coupling, with a correlation of 0.51 (95% significance; not shown in figures), suggesting that the more negative cloud cover responses in some models play a role in the reduced liquid water path response. Understanding negative cloud-cover responses will help to further understand LWP–SST coupling bias because
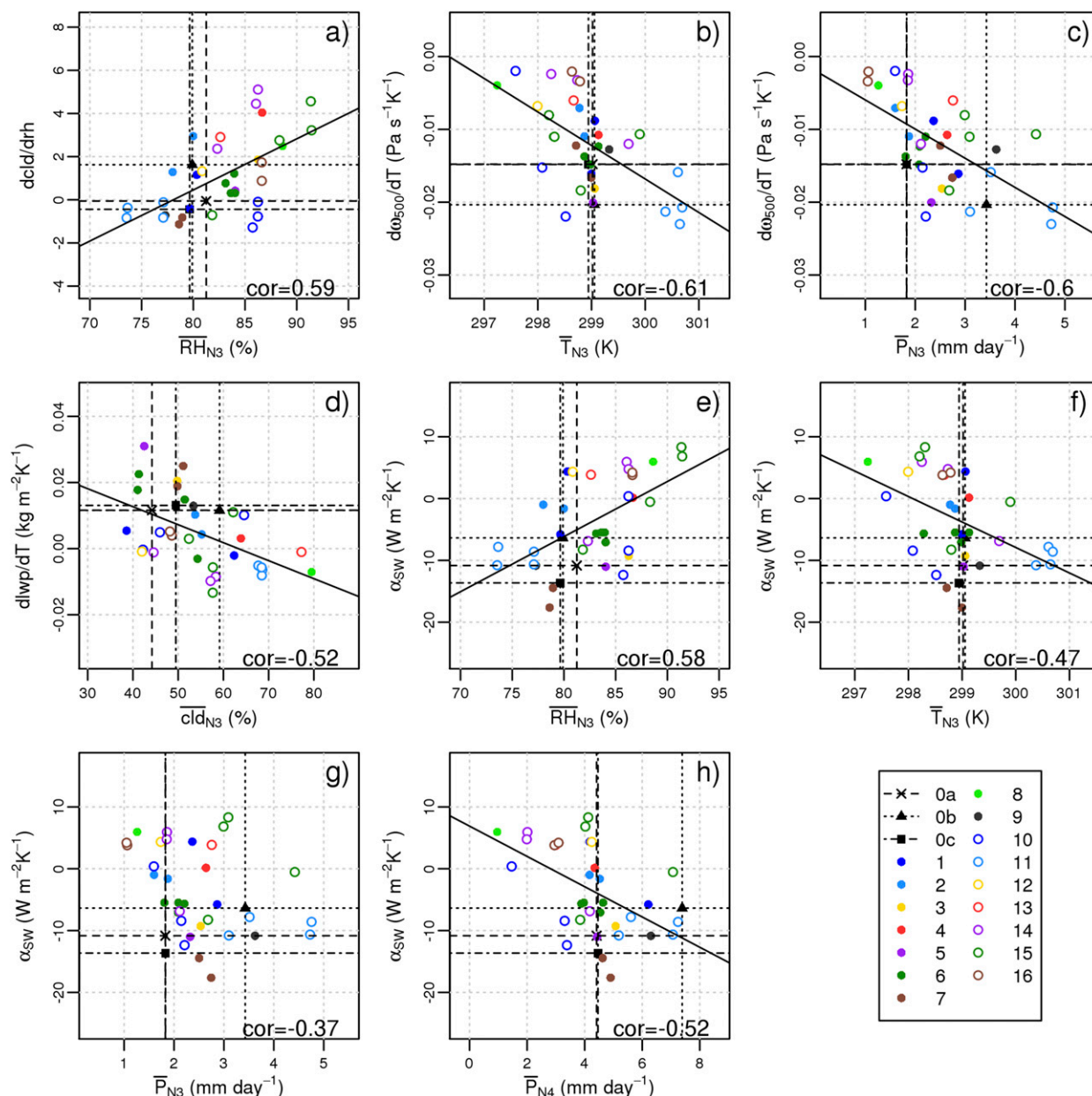
FIG. 7. (a) Cloud–RH coupling plotted against mean Niño-3 relative humidity; (b) ω_{500}–SST coupling against mean Niño-3 SST; (c) ω_{500}–SST coupling against mean Niño-3 precipitation; (d) LWP–SST coupling against mean Niño-3 cloud fraction; (e) SW feedback against mean Niño-3 relative humidity; (f) as in (e), but with mean Niño-3 SST on the x axis; (g) as in (e), but with mean Niño-3 precipitation on the x axis; (h) as in (e), but with mean Niño-4 precipitation on the x axis. Correlations of the relationships for CMIP5 ensemble members are printed on figures. The fitting line indicates a relationship significant at the 95% level (t test). Observational estimates are shown by dashed (ERA-I/OAFlux), dotted (NCEP2), and dot–dashed (MERRA-2) lines.

of this, though errors in cloud water content responses will also play a role. Note that mean total cloud cover is not strongly linked to temperature or precipitation measures of the cold tongue bias. Also, the LWP–SST coupling variation is less related to the total SW feedback than cloud–RH and ω_{500}–SST couplings. Therefore, the Niño-3 mean total cloud cover is not found to

be significantly linked to the total SW feedback (not shown in figures), but rather the horizontal and vertical distribution of the clouds is of importance. For example, in two models where total cloud cover may be the same, a model with relatively more low cloud cover may have a more biased SW feedback than one with relatively more high cloud cover.
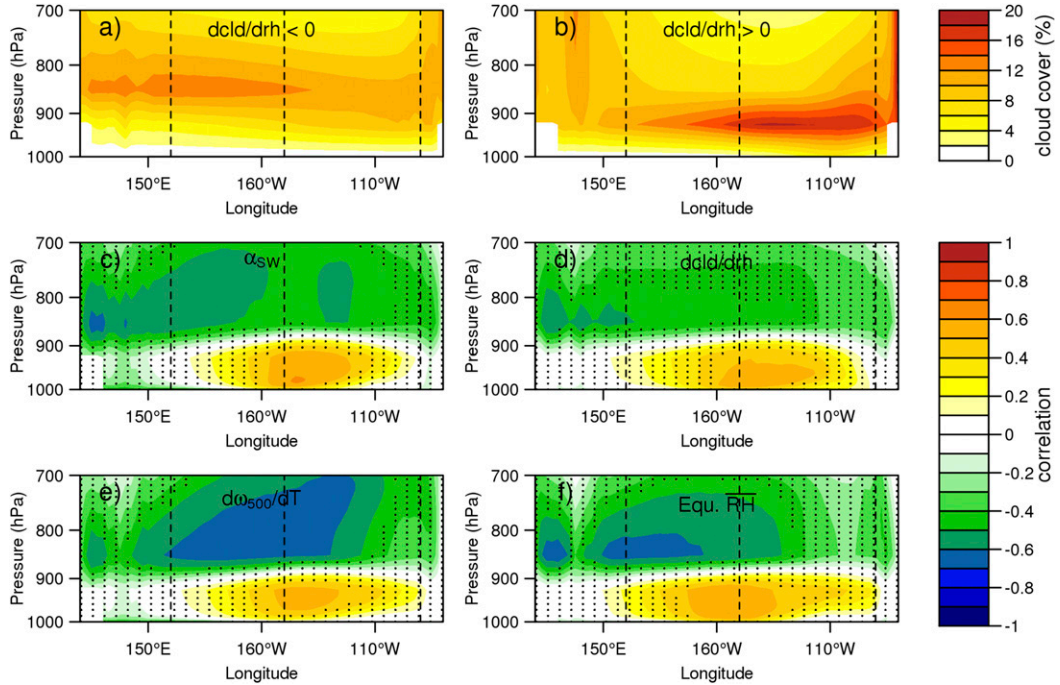
FIG. 8. (a) Mean cloud (%; averaged over latitude 5°S–5°N) for CMIP5 models with negative east Pacific cloud–RH coupling; (b) as in (a), but for CMIP5 models with positive cloud–RH coupling; (c) correlation of CMIP5 time-mean cloud (averaged over latitude 5°S–5°N) at each grid point with CMIP5 east equatorial Pacific SW feedback, α_{SW}; (d) as in (c), but correlated with CMIP5 east equatorial Pacific cloud–RH coupling; (e) as in (c), but correlated with CMIP5 east equatorial Pacific ω_{500}–SST coupling, $d\omega_{500}/dT$; (f) as in (c), but correlated with CMIP5 mean equatorial Pacific (averaged over longitude 160°E–90°W; latitude 5°S–5°N) surface relative humidity. Regions where correlation is below 95% significance (t test) are stippled. Niño-3 and Niño-4 regions are shown using vertical dashed lines.

Ultimately, these results show strong links between the mean equatorial Pacific, including persistent coupled model biases, and ENSO SW feedback processes in the CMIP5 models. In particular, links between the mean climate and cloud–RH coupling may be indicative of the variation in the vertical distribution of cloud over the equatorial Pacific. This can be confirmed by examining the vertical distribution of mean cloud cover over the equatorial Pacific for models with a negative cloud–RH coupling and models with a positive cloud–RH coupling (Figs. 8a,b). A region of more cloud cover between the surface and 900 hPa over the east and central equatorial Pacific exists for models with a positive cloud–RH coupling (Fig. 8b). By comparison, models with a negative cloud–RH coupling (Fig. 8a) have more cloud at slightly higher altitudes (900–800 hPa), farther toward the west. There is relatively less low cloud over the east equatorial Pacific, where cloud–RH coupling is important to SW feedback.

The relationship between SW feedback and the distribution of cloud is also extended in Fig. 8c, where CMIP5 Niño-3 SW feedback is correlated with mean cloud cover at each grid point. A positive correlation is found nearer

the surface in the east equatorial Pacific, showing that models with more cloud in this location have a more positive SW feedback. Conversely, more cloud cover at higher altitudes toward the west is present in models with a stronger negative SW feedback. This relationship persists for both the dominant SW feedback components, cloud–RH and ω_{500}–SST couplings (Figs. 8d,e). This indicates that variation in both the vertical and the zonal distribution of cloud is linked to differences in the SW feedback regime. For example, models with more low cloud in the east equatorial Pacific tend to have weaker ω_{500}–SST coupling, reducing DY. The cloud–RH coupling also tends to be more positive, resulting in a stronger positive RHF. Therefore, the positive regime of SW feedback is more dominant; the stratiform clouds are broken up during El Niño events as a result of decreased static stability, and more shortwave radiation reaches the surface, warming the SSTs. Conversely, the negative regime of SW feedback driven by dynamical processes is more dominant in models with more cloud cover in the west and less low cloud in the east. Clouds form in the central and east equatorial Pacific during El Niño events and block the incoming shortwave radiation, cooling the SSTs.

The mean surface relative humidity in the equatorial Pacific is found to be a relatively good indicator of the distribution of clouds (Fig. 8f) and the strength of El Niño SW feedback. Models with more surface relative humidity are those with a larger amount of cloud nearer the surface in the east equatorial Pacific, as shown by the region of positive correlation, and less cloud cover in the west. This explains the relationships shown in Fig. 8a and Fig. 8e and provides a useful metric for this variation in vertical cloud distribution in CMIP5. These results provide information regarding the variation of cloud cover in relation to El Niño feedbacks in CMIP5 models but do not confirm that mean cloud and cloud responses are linked to SW feedback bias in comparison to observations.

Vertical distribution of cloud is not easily comparable to ISCCP, as observation methods complicate comparison. However, there have been efforts made as part of the Cloud Feedback Model Intercomparison Project phase 1 and phase 2 (CFMIP1 and CFMIP2; McAvaney and LeTreut 2003; Bony et al. 2011) to replicate the measurement of cloud properties in ISCCP for CMIP5 model cloud (ISCCP simulator; Klein and Jakob 1999; Webb et al. 2001). Therefore, cloud analysis is also carried out on ISCCP cloud area fraction for six of the CMIP5 models for which diagnostics are available (indicated in Table 1) to directly compare CMIP5 cloud with ISCCP observations (not shown in figures) as a means to assess cloud bias in CMIP5. It is found that, in those six models, there is a tendency for more mean cloud than observed in the Niño-3 region over 1000–800 hPa. Similarly, regressing 1000–800-hPa cloud anomalies onto Niño-3 surface relative humidity anomalies shows that the cloud–RH coupling in this region is too strong in the three models that also have a total cloud–RH coupling that is too strong: both MIROC-ESM models and CanESM2. Therefore, bias in low cloud responses is a contributor to the total cloud-cover response bias, and hence the SW damping bias, in those models. Conversely, the remaining three models, HadGEM2-ES, MIROC5, MRI-CGCM3, that do not have total cloud–RH coupling with significant biases also have no significant bias in low cloud–RH coupling.

c. Diagnosing sources of El Niño shortwave feedback bias

To gain greater insight into the underlying causes of SW feedback bias, the AMIP runs are also examined. In these runs, observed varying SSTs are prescribed to the atmosphere models. This means that mean-SST and El Niño–related SSTAs in the AMIP models are the same as those observed. Feedback calculation in AMIP therefore represents the atmospheric response to SSTAs

but has no feedback on the SST. Figure 9 compares the CMIP and AMIP SW feedback for 15 models of the CMIP5 ensemble. SW feedback is still significantly weak in AMIP compared to the observations for a number of the models (Fig. 9a). In particular, cloud–ω_{500} coupling and SW flux–cloud coupling are significantly weak for 12 of the AMIP models (not shown). However, SW feedback can also have significant differences between CMIP and AMIP, mainly in the models that have a positive SW feedback regime in the coupled models (MRI-CGCM3, ACCESS1.3, INM-CM4.0, IPSL-CM5A-MR, IPSL-CM5A-LR, CSIRO Mk3.6.0). These models tend to show a change to a more negative SW feedback from CMIP to AMIP. This is a result of increased DY (Fig. 9b), slightly reduced RHF (Fig. 9c), and more negative LWPF (Fig. 9d) in AMIP, compared to CMIP. Feedback changes from AMIP to CMIP contribute to a more accurate SW feedback; no models have a significantly more biased SW feedback in AMIP when compared to the corresponding CMIP model feedback. It is possible that reduced bias in SW feedbacks in AMIP is a result of prescribed SSTs, following the relationships demonstrated in Fig. 7. More accurate mean SSTs may minimize mean atmospheric circulation biases and biases in atmospheric circulation responses during El Niño events (i.e., the ω_{500}–SST coupling). This can be tested by examining differences in the mean state from CMIP to AMIP and relationships they may have to the corresponding difference in SW feedback.

The differences in SW feedback from CMIP to AMIP are mainly driven by differences in the ω_{500}–SST coupling, the dominant component of the DY feedback (Fig. 10a). Models that have the largest bias reduction in SW feedback from CMIP to AMIP are those that have larger differences in the ω_{500}–SST coupling between AMIP and CMIP (correlation of 0.90). Further to this, differences between AMIP and CMIP in ω_{500}–SST coupling can be linked to mean state differences. The largest differences in ω_{500}–SST coupling coincide with more Niño-3 Pacific precipitation (Fig. 10b; correlation of −0.65) and increased atmospheric ascent (Fig. 10c; correlation of 0.77) in AMIP. These tend to be the models that have larger mean state biases in the coupled runs (Fig. 4). This implies that the models with larger feedback biases and mean state biases in the coupled runs are improved in the atmosphere-only runs, and are linked to the larger SW feedback changes in those models (Fig. 9). It is also noted that a number of the models with the largest differences between AMIP and CMIP in SW feedback and ω_{500}–SST coupling have less Niño-3.4 low cloud in the corresponding AMIP runs (Figs. 10d,h) that is linked to the positive SW feedback in the coupled runs (Fig. 8c). Niño-3.4, calculated using longitude range 170°–120°W, is
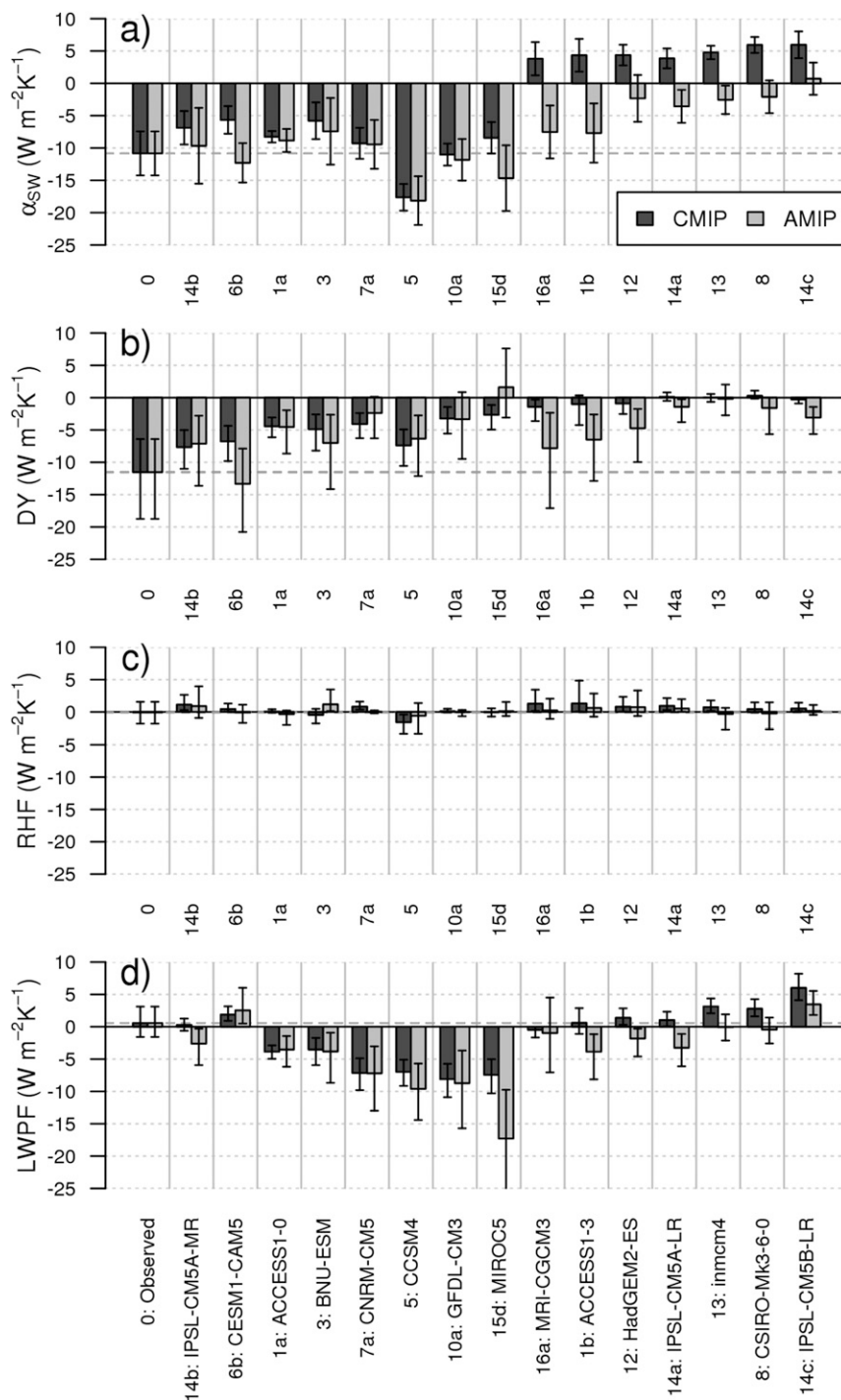
FIG. 9. CMIP5 (dark gray bars) and AMIP (light gray bars) El Niño (a) shortwave feedback (regression of Niño-3 Q_{SW} anomalies against Niño-3 SSTA for SSTA > 0), (b) DY, (c) RHF, and (d) LWPF. Error bars indicate the 95% confidence intervals in the linear fits used in the feedback calculation. Horizontal dashed line shows observational estimate using ERA-I/OAFlux.
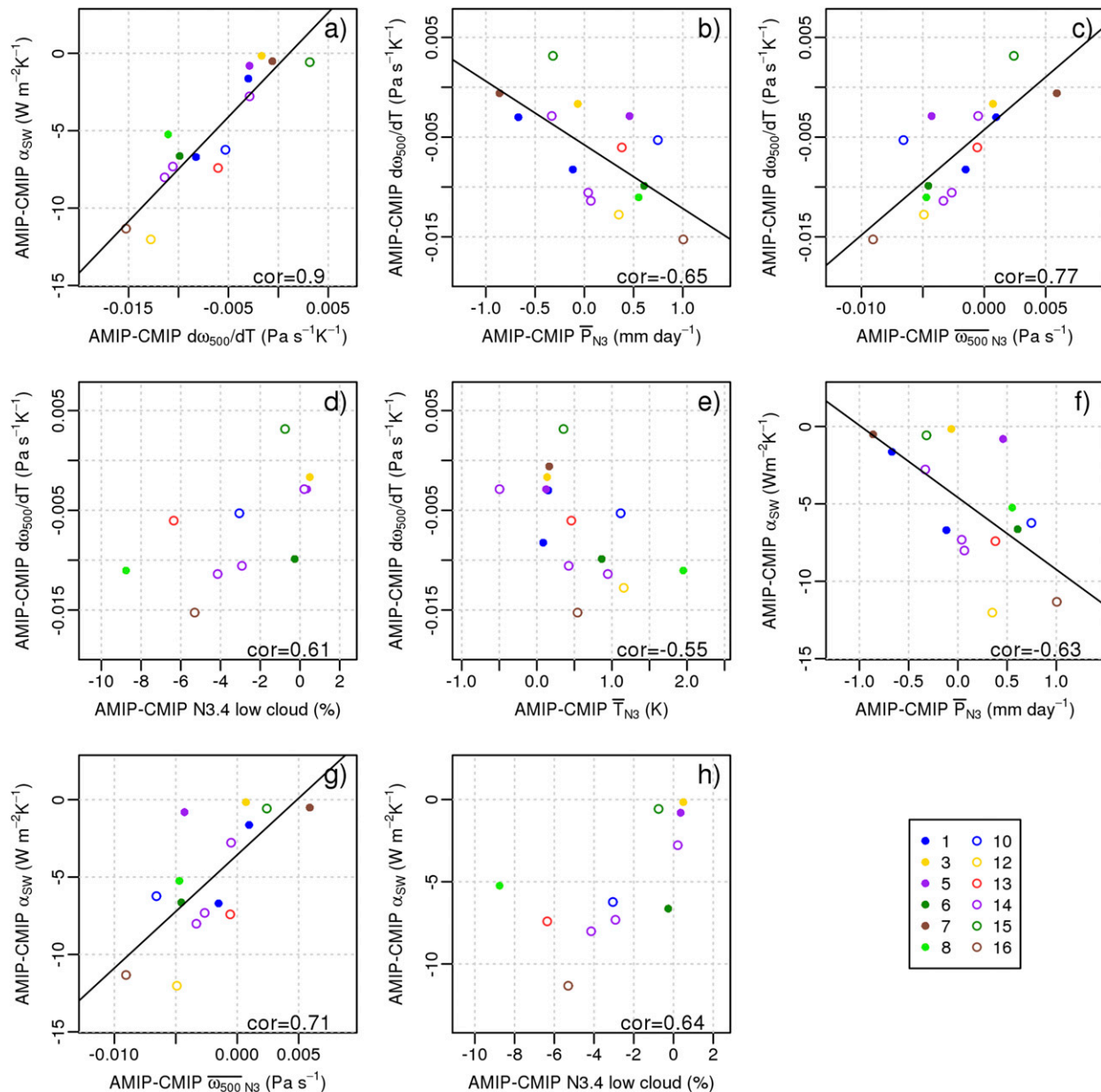
FIG. 10. (a) AMIP minus CMIP SW feedback, α_{SW}, plotted against AMIP minus CMIP ω_{500}–SST coupling; (b) AMIP minus CMIP ω_{500}–SST coupling against AMIP minus CMIP mean Niño-3 precipitation; (c) as in (b), but with mean Niño-3 ω_{500} on the x axis; (d) as in (b), but with mean Niño-3.4 low cloud fraction (cloud averaged over 1000–900 hPa) on the x axis; (e) as in (b), but with mean Niño-3 SST on the x axis; (f) as in (b), but with SW feedback on the y axis; (g) as in (c), but with SW feedback on the y axis; (h) as in (d), but with SW feedback on the y axis. Correlations of the relationships are printed on figures. The fitting line indicates a relationship significant at the 95% level (t test).

used for low cloud in Fig. 10 in order to fully capture the region of importance in Fig. 8.

There is a weaker link between the AMIP–CMIP changes in ω_{500}–SST coupling and changes in mean Niño-3 SST (Fig. 10e). This is perhaps unexpected given that the SSTs are prescribed in AMIP, eliminating SST bias; the AMIP–CMIP difference in mean Niño-3 SST is

simply the CMIP5 bias. This may be expected to be linked to biases in atmospheric circulation and in the ω_{500}–SST coupling, given the strong interensemble relationship in the coupled models (Fig. 7b). However, the relationship between CMIP5 mean SST and CMIP5 ω_{500}–SST coupling for the subset of models available for AMIP analysis is less strong (correlation of -0.46) than

for the full CMIP5 ensemble. It is possible this is a cause of this weaker relationship between AMIP–CMIP ω_{500}–SST coupling and mean SST.

Note that AMIP-only feedback biases are not strongly linked to the AMIP-only mean state (not shown in figures), perhaps as a result of less variation in the mean state in AMIP models compared with CMIP5. Very accurate SSTs in AMIP, as all the models have by design, does not mean that the SW feedbacks are also as accurate, despite the link between mean SST and SW feedback when models are coupled. However, outlier INM-CM4.0 is a cause of some of the weak relationships. Removing this model from analysis significantly increases the link between mean Niño-3 precipitation and ω_{500}–SST coupling (correlation of -0.81). This is a result of this model having very excessive mean precipitation along the equator in AMIP; INM-CM4.0 has $7.22\,\mathrm{mm\,day}^{-1}$ in Niño-4 and $3.14\,\mathrm{mm\,day}^{-1}$ in Niño-3 compared to 4.41 and $1.83\,\mathrm{mm\,day}^{-1}$ in GPCP. This then means the convective response is suppressed during El Niño events in this model.

It would be very useful for model development if one could predict the magnitude of coupled model bias from some analysis of the atmosphere-only simulation. Unfortunately, no significant relationships are found between the mean state conditions and feedbacks in AMIP with the AMIP–CMIP difference in feedbacks. Nonetheless, a number of the more biased CMIP5 models are significantly biased in AMIP and showed larger differences between AMIP and CMIP runs, highlighting the importance of minimizing bias in atmosphere models. These relationships also reinforce the link between biases in equatorial Pacific mean conditions and El Niño feedback strength.

This helps to explain more significant differences for a number of the models in El Niño feedbacks between AMIP and CMIP. However, Fig. 9 does show that almost all of the models that have negative SW feedbacks in the coupled models have no significant difference in SW feedback in AMIP compared to CMIP. An exception to this is CESM1(CAM5), which has a stronger SW feedback in AMIP as a result of stronger DY. In general, difference in El Niño SW feedbacks between AMIP and CMIP is relatively small. Indeed, the AMIP and CMIP SW feedbacks are significantly related. Correlations of 0.89, 0.58, and 0.86 (95% significant) are found between CMIP and AMIP SW feedback, DY, and LWPF, respectively (not shown in figures). The relationship between CMIP and AMIP RHF is low (correlation of 0.38). However, if ACCESS1.0 is excluded this is increased to 0.71.

Results suggest that for many of these CMIP5 models, the bias in SW feedback is strongly linked to biases in the corresponding atmosphere model. In particular, biases in cloud-related processes, such as the SW–cloud coupling, the cloud–ω_{500} coupling, and the LWP–SST coupling, persist in AMIP and result in SW feedback bias (not shown in figures). It is possible these underlying feedback biases are related to convection schemes (Neale et al. 2008; Guilyardi et al. 2009; Watanabe et al. 2011; Kim et al. 2011) or atmosphere model resolution (Hack et al. 2006; Sun et al. 2006; Li and Zhang 2008) and are consequently less affected by the prescribed SSTs. However, from this study it has not been possible to attribute SW feedback bias to differences in atmospheric resolution or convection scheme, and it is not possible in a study such as this to isolate a single source of bias, as such convection schemes and atmosphere model properties are inherently linked.

5. Summary and discussion

The CMIP5 ensemble has a large range in the strength of shortwave feedback during El Niño events, with models demonstrating both positive and negative feedbacks. Here, additional insight is gained into underlying mechanisms of shortwave feedback bias by linking variations in cloud-cover responses that drive shortwave feedback variation to common CMIP5 mean state biases in the equatorial Pacific, such as cool SSTs along the equator and spatial variations in mean state atmospheric circulation and clouds.

Variation among CMIP5 models in shortwave feedback is most strongly linked to a component of the dynamical cloud feedback, the ω_{500}–SST coupling, and a component of the relative humidity cloud feedback, the cloud–RH coupling. These components are linked to one another, demonstrating two "regimes" of shortwave feedback, negative and positive, that are described by the idealized schematics in Fig. 11. The positive cloud–RH coupling represents a breakup of stratiform clouds during El Niño events that consequently increases surface downward shortwave heat flux (see schematics in Figs. 11c,d); the negative ω_{500}–SST coupling represents increasing atmospheric ascent during El Niño events that causes convective clouds and reduced surface shortwave heat flux (see schematic in Figs. 11a,b).

These components of the shortwave feedback, the ω_{500}–SST coupling and cloud–RH coupling, are significantly linked to biases in the mean equatorial Pacific climate in the CMIP5 models. A stronger positive cloud–RH coupling dominates in models that have higher surface relative humidity and more low cloud in the east equatorial Pacific. This low cloud is then broken up during El Niño events causing the incoming shortwave radiation to reach the surface of the ocean.
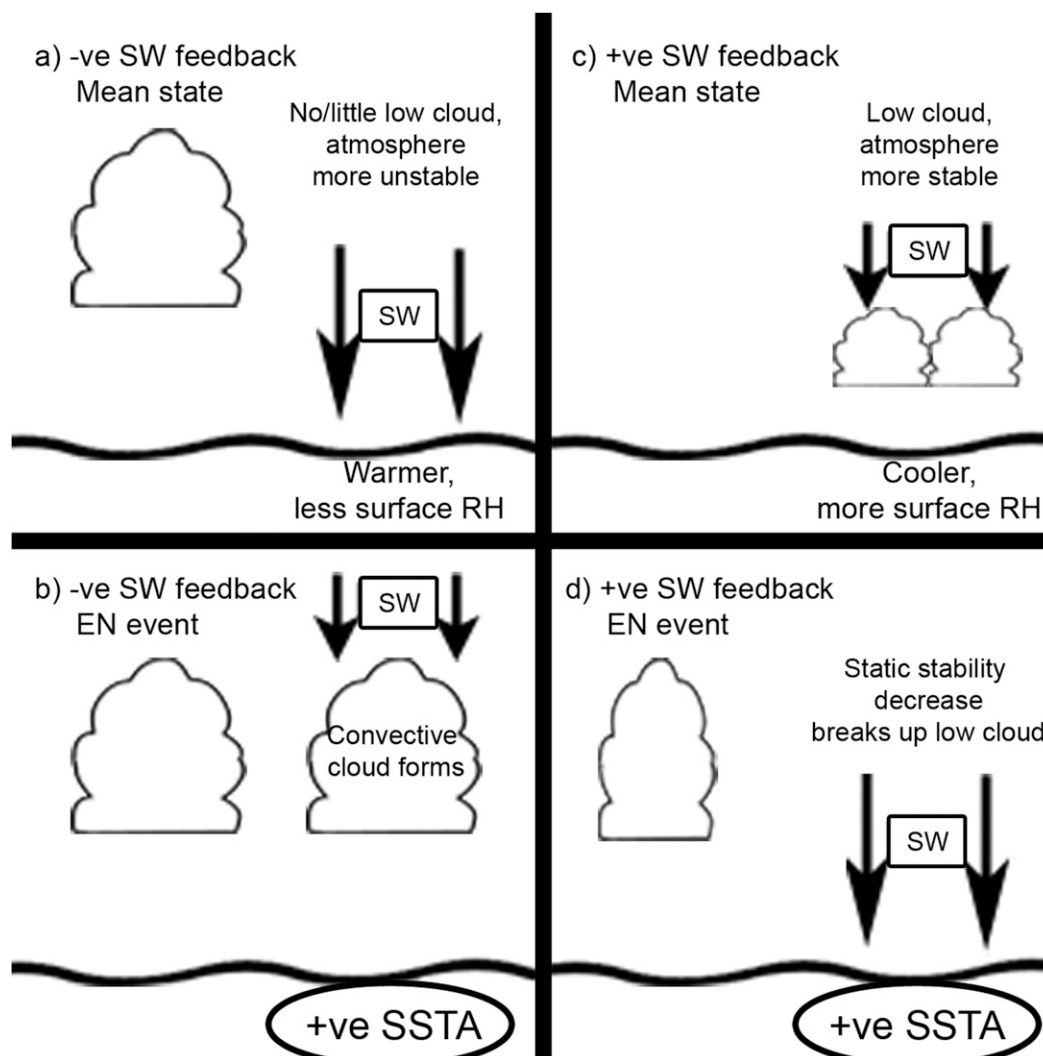
FIG. 11. Idealized schematics of the equatorial Pacific showing (a) mean state conditions for models with negative SW feedback, (b) El Niño conditions for models with negative SW feedback, (c) mean state conditions for models with positive SW feedback, and (d) El Niño conditions for models with positive SW feedback.

Conversely, those models with warmer equatorial Pacific SSTs, more equatorial precipitation, and less low cloud in Niño-3 have a stronger ω_{500}–SST coupling, and therefore a more negative shortwave feedback. While these results highlight the importance of the mean state in coupled models in relation to El Niño atmospheric feedbacks, the mean state biases discussed here are undoubtedly linked, and it is not possible to use results such as these to determine an underlying cause of mean state bias. Indeed, understanding the initial cause of such biases is a substantial ongoing area of research.

Changes in the mean state atmospheric circulation and cloud properties in the equatorial Pacific between CMIP and AMIP can also be related to changes in the ω_{500}–SST coupling that result in changes in shortwave feedback, namely a change from a positive shortwave feedback to a negative shortwave feedback in a number of models. This importance of ω_{500}–SST coupling is consistent with the interensemble relationships found and a study of previous-generation coupled models (CMIP3) by Lloyd et al. (2012). This is perhaps unsurprising as the dynamical response is driven by prescribed SSTs in AMIP but provides a feedback on the ocean in coupled models. However, AMIP analysis shows that a number of models have no significant difference in the shortwave feedback compared with CMIP5 analysis, suggesting that bias in the atmosphere model plays an important role in shortwave feedback and mean state bias.

Biases in shortwave feedback are also related to longwave feedback due to the influence of clouds on both heat fluxes. There exists a correlation of -0.89 between the two, such that bias in longwave feedback tends to compensate for bias in shortwave feedback. However, the magnitude of longwave feedback bias tends to be smaller, so a net positive thermodynamic damping bias still remains. This demonstrates how the relative contribution of El Niño atmospheric feedbacks to event damping can also be linked to the mean state.

Results found in this study can be used in combination with the study of ENSO latent heat damping by Ferrett et al. (2017) to gain a more complete understanding of El Niño thermodynamic damping in relation to the mean climate in current coupled models. Figure 1b demonstrates that latent heat feedback and shortwave feedback are related. Mean Niño-4 surface relative humidity, found here to be strongly linked to shortwave feedback, is also related to the precipitation metric for the double-ITCZ bias used by Ferrett et al. (2017); mean precipitation area averaged over longitude 150°–90°W and latitude 15°–5°S (correlation of -0.68; not shown in figures). Therefore, both the cold tongue bias and the double-ITCZ bias can be linked to errors in El Niño thermodynamic damping.

Both studies also find that errors in El Niño thermodynamic damping can be traced back to the atmosphere component of the coupled model. Furthermore, the strong links between mean state and feedback drifts introduced by coupling in some models may also be of particular importance. While no significant relationships are found between the AMIP mean state and shortwave feedbacks with the AMIP–CMIP change in shortwave feedbacks, a number of the most biased models showed larger shortwave feedback differences between AMIP and CMIP runs. These models also tend to be significantly biased in AMIP. This may indicate that modifications developed to improve the atmosphere component can be directly translated to improvements in the coupled model simulation of ENSO.

REFERENCES

AchutaRao, K., and K. R. Sperber, 2006: ENSO simulation in coupled ocean-atmosphere models: Are the current models better? *Climate Dyn.*, **27**, 1–15, https://doi.org/10.1007/s00382-006-0119-7.

Adler, R. F., and Coauthors, 2003: The Version-2 Global Precipitation Climatology Project (GPCP) monthly precipitation analysis (1979–present). *J. Hydrometeor.*, **4**, 1147–1167, https://doi.org/10.1175/1525-7541(2003)004<1147:TVGPCP>2.0.CO;2.

Bellenger, H., E. Guilyardi, J. Leloup, M. Lengaigne, and J. Vialard, 2014: ENSO representation in climate models: From CMIP3 to CMIP5. *Climate Dyn.*, **42**, 1999–2018, https://doi.org/10.1007/s00382-013-1783-z.

Bjerknes, J., 1969: Atmospheric teleconnections from the equatorial Pacific. *Mon. Wea. Rev.*, **97**, 163–172, https://doi.org/10.1175/1520-0493(1969)097<0163:ATFTEP>2.3.CO;2.

Bony, S., M. Webb, C. Bretherton, S. Klein, P. Siebesma, G. Tselioudis, and M. Zhang, 2011: CFMIP: Towards a better evaluation and understanding of clouds and cloud feedbacks in CMIP5 models. *CLIVAR Exchanges*, No. 56, International CLIVAR Project Office, Southampton, United Kingdom, 20–24.

Cai, W., and Coauthors, 2014: Increasing frequency of extreme El Niño events due to greenhouse warming. *Nat. Climate Change*, **4**, 111–116, https://doi.org/10.1038/nclimate2100.

Capotondi, A., A. Wittenberg, and S. Masina, 2006: Spatial and temporal structure of tropical Pacific interannual variability in 20th century coupled simulations. *Ocean Modell.*, **15**, 274–298, https://doi.org/10.1016/j.ocemod.2006.02.004.

Chen, L., Y. Yu, and D. Sun, 2013: Cloud and water vapor feedbacks to the El Niño warming: Are they still biased in CMIP5 models? *J. Climate*, **26**, 4947–4961, https://doi.org/10.1175/JCLI-D-12-00575.1.

——, T. Li, and Y. Yu, 2015: Causes of strengthening and weakening of ENSO amplitude under global warming in four CMIP5 models. *J. Climate*, **28**, 3250–3274, https://doi.org/10.1175/JCLI-D-14-00439.1.

——, ——, ——, and S. K. Behera, 2017: A possible explanation for the divergent projection of ENSO amplitude change under global warming. *Climate Dyn.*, **49**, 3799–3811, https://doi.org/10.1007/s00382-017-3544-x.

de Szoeke, S. P., and S. Xie, 2008: The tropical eastern Pacific seasonal cycle: Assessment of errors and mechanisms in IPCC AR4 coupled ocean–atmosphere general circulation models. *J. Climate*, **21**, 2573–2590, https://doi.org/10.1175/2007JCLI1975.1.

Dee, D. P., and Coauthors, 2011: The ERA-Interim reanalysis: Configuration and performance of the data assimilation system. *Quart. J. Roy. Meteor. Soc.*, **137**, 553–597, https://doi.org/10.1002/qj.828.

Ferrett, S., and M. Collins, 2016: ENSO feedbacks and their relationships with the mean state in a flux adjusted ensemble. *Climate Dyn.*, https://doi.org/10.1007/s00382-016-3270-9, in press.

——, ——, and H.-L. Ren, 2017: Understanding bias in the evaporative damping of El Niño–Southern Oscillation events in CMIP5 models. *J. Climate*, **30**, 6351–6370, https://doi.org/10.1175/JCLI-D-16-0748.1.

Gelaro, R., and Coauthors, 2017: The Modern-Era Retrospective Analysis for Research and Applications, version 2 (MERRA-2). *J. Climate*, **30**, 5419–5454, https://doi.org/10.1175/JCLI-D-16-0758.1.

Guilyardi, E., P. Braconnot, F.-F. Jin, S. T. Kim, M. Kolasinski, T. Li, and I. Musat, 2009: Atmosphere feedbacks during ENSO in a coupled GCM with a modified atmospheric convection scheme. *J. Climate*, **22**, 5698–5718, https://doi.org/10.1175/2009JCLI2815.1.

Hack, J., J. Caron, G. Danabasoglu, K. Oleson, C. Bitz, and J. Truesdale, 2006: CCSM–CAM3 climate simulation sensitivity to changes in horizontal resolution. *J. Climate*, **19**, 2267–2289, https://doi.org/10.1175/JCLI3764.1.

Jin, F.-F., S. T. Kim, and L. Bejarano, 2006: A coupled-stability index of ENSO. *Geophys. Res. Lett.*, **33**, L23708, https://doi.org/10.1029/2006GL027221.

Kanamitsu, M., W. Ebisuzaki, J. Woollen, S.-K. Yang, J. Hnilo, M. Fiorino, and G. Potter, 2002: NCEP–DOE AMIP-II Reanalysis (R-2). *Bull. Amer. Meteor. Soc.*, **83**, 1631–1643, https://doi.org/10.1175/BAMS-83-11-1631.

Kim, D., Y.-S. Jang, D.-H. Kim, Y. H. Kim, M. Watanabe, F.-F. Jin, and J. S. Kug, 2011: El Niño–Southern Oscillation sensitivity to cumulus entrainment in a coupled general circulation model. *J. Geophys. Res.*, **116**, D22112, https://doi.org/10.1029/2011JD016526.

Kim, S. T., and F.-F. Jin, 2011a: An ENSO stability analysis. Part I: Results from a hybrid coupled model. *Climate Dyn.*, **36**, 1593–1607, https://doi.org/10.1007/s00382-010-0796-0.

——, and ——, 2011b: An ENSO stability analysis. Part II: Results from the twentieth and twenty-first century simulations of the CMIP3 models. *Climate Dyn.*, **36**, 1609–1627, https://doi.org/10.1007/s00382-010-0872-5.

——, W. Cai, F.-F. Jin, and J.-Y. Yu, 2014a: ENSO stability in coupled climate models and its association with mean state. *Climate Dyn.*, **42**, 3313–3321, https://doi.org/10.1007/s00382-013-1833-6.

——, ——, ——, A. Santoso, L. Wu, E. Guilyardi, and S.-I. An, 2014b: Response of El Niño sea surface temperature variability to greenhouse warming. *Nat. Climate Change*, **4**, 786–790, https://doi.org/10.1038/nclimate2326.

Klein, S. A., and D. L. Hartmann, 1993: The seasonal cycle of low stratiform clouds. *J. Climate*, **6**, 1587–1606, https://doi.org/10.1175/1520-0442(1993)006<1587:TSCOLS>2.0.CO;2.

——, and C. Jakob, 1999: Validation and sensitivities of frontal clouds simulated by the ECMWF model. *Mon. Wea. Rev.*, **127**, 2514–2531, https://doi.org/10.1175/1520-0493(1999)127<2514:VASOFC>2.0.CO;2.

Li, G., and G. J. Zhang, 2008: Understanding biases in shortwave cloud radiative forcing in the National Center for Atmospheric Research Community Atmosphere Model (CAM3) during El Niño. *J. Geophys. Res.*, **113**, D02103, https://doi.org/10.1029/2008JE003097.

——, and S. Xie, 2014: Tropical biases in CMIP5 multimodel ensemble: The excessive equatorial Pacific cold tongue and double ITCZ problems. *J. Climate*, **27**, 1765–1780, https://doi.org/10.1175/JCLI-D-13-00337.1.

Li, L. J., B. Wang, and G. J. Zhang, 2014: The role of nonconvective condensation processes in response of surface shortwave cloud radiative forcing to El Niño warming. *J. Climate*, **27**, 6721–6736, https://doi.org/10.1175/JCLI-D-13-00632.1.

——, ——, and ——, 2015: The role of moist processes in shortwave radiative feedback during ENSO in the CMIP5 models. *J. Climate*, **28**, 9892–9908, https://doi.org/10.1175/JCLI-D-15-0276.1.

Lin, J., 2007: The double-ITCZ problem in IPCC AR4 coupled GCMs: Ocean–atmosphere feedback analysis. *J. Climate*, **20**, 4497–4525, https://doi.org/10.1175/JCLI4272.1.

Lloyd, J., E. Guilyardi, H. Weller, and J. Slingo, 2009: The role of atmosphere feedbacks during ENSO in the CMIP3 models. *Atmos. Sci. Lett.*, **10**, 170–176, https://doi.org/10.1002/asl.227.

——, ——, and ——, 2012: The role of atmosphere feedbacks during ENSO in the CMIP3 models. Part III: The shortwave flux feedback. *J. Climate*, **25**, 4275–4293, https://doi.org/10.1175/JCLI-D-11-00178.1.

McAvaney, B. J., and H. Le Treut, 2003: The Cloud Feedback Intercomparison Project: (CFMIP). *CLIVAR Exchanges*, No. 26, International CLIVAR Project Office, Southampton, United Kingdom, 1–4.

Mechoso, C. A., and Coauthors, 1995: The seasonal cycle over the tropical Pacific in coupled ocean–atmosphere general circulation models. *Mon. Wea. Rev.*, **123**, 2825–2838, https://doi.org/10.1175/1520-0493(1995)123<2825:TSCOTT>2.0.CO;2.

Neale, R., J. Richter, and M. Jochum, 2008: The impact of convection on ENSO: From a delayed oscillator to a series of events. *J. Climate*, **21**, 5904–5924, https://doi.org/10.1175/2008JCLI2244.1.

Philander, S., D. Gu, G. Lambert, T. Li, D. Halpern, N.-C. Lau, and R. C. Pacanowski, 1996: Why the ITCZ is mostly north of the equator. *J. Climate*, **9**, 2958–2972, https://doi.org/10.1175/1520-0442(1996)009<2958:WTIIMN>2.0.CO;2.

Ramanathan, V., and W. Collins, 1991: Thermodynamic regulation of ocean warming by cirrus clouds deduced from observations of the 1987 El Niño. *Nature*, **351**, 27–32, https://doi.org/10.1038/351027a0.

Schiffer, R. A., and W. B. Rossow, 1983: The International Satellite Cloud Climatology Project (ISCCP): The first project of the World Climate Research Programme. *Bull. Amer. Meteor. Soc.*, **64**, 779–784.

Sun, D.-Z., J. Fasullo, T. Zhang, and A. Roubicek, 2003: On the radiative and dynamical feedbacks over the equatorial cold tongue. *J. Climate*, **16**, 2425–2432, https://doi.org/10.1175/2786.1.

——, and Coauthors, 2006: Radiative and dynamical feedbacks over the equatorial cold tongue: Results from nine atmospheric GCMs. *J. Climate*, **19**, 4059–4074, https://doi.org/10.1175/JCLI3835.1.

——, Y. Yu, and T. Zhang, 2009: Tropical water vapor and cloud feedbacks in climate models: A further assessment using coupled simulations. *J. Climate*, **22**, 1287–1304, https://doi.org/10.1175/2008JCLI2267.1.

Taylor, K. E., R. J. Stouffer, and G. A. Meehl, 2012: An overview of CMIP5 and the experiment design. *Bull. Amer. Meteor. Soc.*, **93**, 485–498, https://doi.org/10.1175/BAMS-D-11-00094.1.

Vannière, B., E. Guilyardi, G. Madec, F. Doblas-Reyes, and S. Woolnough, 2013: Using seasonal hindcasts to understand the origin of the equatorial cold tongue bias in CGCMs and its impact on ENSO. *Climate Dyn.*, **40**, 963–981, https://doi.org/10.1007/s00382-012-1429-6.

——, ——, T. Toniazzo, G. Madec, and S. Woolnough, 2014: A systematic approach to identify the sources of tropical SST errors in coupled models using the adjustment of initialised experiments. *Climate Dyn.*, **43**, 2261–2282, https://doi.org/10.1007/s00382-014-2051-6.

Watanabe, M., M. Chikira, Y. Imada, and M. Kimoto, 2011: Convective control of ENSO simulated in MIROC. *J. Climate*, **24**, 543–562, https://doi.org/10.1175/2010JCLI3878.1.

Webb, M., C. Senior, S. Bony, and J. J. Morcrette, 2001: Combining ERBE and ISCCP data to assess clouds in the Hadley Centre, ECMWF and LMD atmospheric climate models. *Climate Dyn.*, **17**, 905–922, https://doi.org/10.1007/s003820100157.

Yu, L., and R. A. Weller, 2007: Objectively analyzed air–sea heat fluxes for the global ice-free oceans (1981–2005). *Bull. Amer. Meteor. Soc.*, **88**, 527–539, https://doi.org/10.1175/BAMS-88-4-527.

Zhang, W., F.-F. Jin, J. Zhao, and J. Li, 2013: On the bias in simulated ENSO SSTA meridional widths of CMIP3 models. *J. Climate*, **26**, 3173–3186, https://doi.org/10.1175/JCLI-D-12-00347.1.

Zhang, X., H. Liu, and M. Zhang, 2015: Double ITCZ in coupled ocean-atmosphere models: From CMIP3 to CMIP5. *Geophys. Res. Lett.*, **42**, 8651–8659, https://doi.org/10.1002/2015GL065973.